ChemComm

Accepted Manuscript

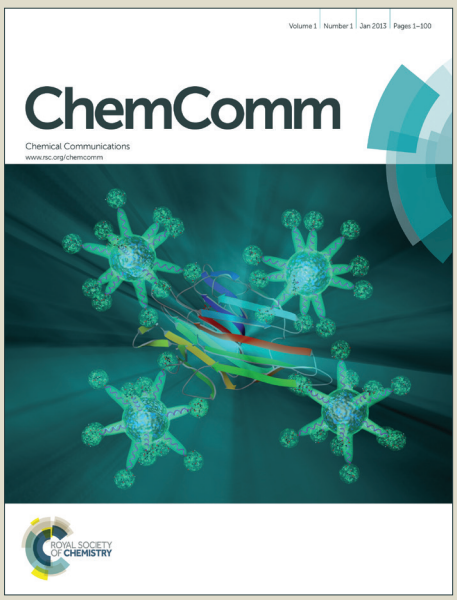

ROYAL SOCIETY OF CHEMISTRY

www.rsc.org/chemcomm

Chemcomm RSCPublishing

COMMUNICATION

Facile Synthesis of PdPt Nanoalloys with Sub-2.0 nm Islands as Robust Electrocatalysts for Methanol Oxidation

Cite this: DOI: 10.1039/x0xx00000x

Received 00th January 2012,
Accepted 00th January 2012

DOI: 10.1039/x0xx00000x

www.rsc.org/chemcomm

Da-Bing Huang,[a] QiangYuan,*[a] Hong-Hui Wang[b] and Zhi-You Zhou*[b]

Composition-tunable PdPt bimetallic nanoalloys with Sub-2.0 nm islands have been successfully synthesized through a facile aqueous solution approach. Among them, the $Pd_{50}Pt_{50}$ nanoalloys exhibit much higher catalytic activity and durability for the methanol oxidation reaction than commercial Pt black.

Recent years, the direct methanol fuel cells (DMFCs) have attracted much research interest as they are promising candidates for providing clean energy and using in portable devices.[1-3]It is well known that Pt is the best catalyst of all pure metals for low-temperature DMFCs. However, the rare reserves and rising price of Pt bring about the obstacle for the widespread development of the methanol fuel cell technology. On the other hand, the poor reaction kinetics and the decrease of catalytic activity over time of pure Pt catalyst also limit the practical large-scale commercialization of DMFCs. In order to overcome these problems, a variety of fabrication approaches are designed to prepare Pt-based bimetallic nanomaterials, which has been considered as promising catalysts for DMFCs because of their enhanced catalytic activity rooting in the modification of the electronic structure of surface Pt atoms that triggered by the close proximity exotic metal atoms.[4-13] As a matter of fact, the size, shape, and composition of Pt-based bimetallic nanomaterials are still vital parameters for impacting their catalytic performances.[14-20] For instance, spherical PdPt nanoalloys[7] displayed a composition-dependent catalytic performance for methanol oxidation. PtZn nanoalloys[5] demonstrate a shape-dependent electrocatalytic activity for methanol oxidation. Therefore, in order to develop electrocatalysts with improved catalytic activity and durability, the controllable synthesis of Pt-based bimetallic nanoalloys still remains a significant challenge**.**

Among reported Pt-based bimetallic nanostructures, the dendritic nanostructures have been attracting extensive interest because the unique nanostructures can bring about more catalytic active sites such as corner atoms and boundaries those considered as major active sites in catalytic reaction.[21-24] For instance, the Pt-on-Pd nanodendrites[21, 22] via two-step, seed-mediated epitaxial growth method reported by Xia's and Yang's groups have displayed significantly enhanced activity and stability towards oxygen reduction reaction. The Pt-on-Pd nanodendrites synthesized through a one-step synthetic method reported by Yamauchi's group[23] exhibit enhanced activity and stability for methanol electrooxidation. However, it still remains a great challenge to design a rational, economic, and environmentally friendly approach to fabricate PdPt nanoalloys with many active sites such as corners, steps and boundaries.

Here, we report a facile aqueous method to directly prepare high-yield PdPt nanoalloys with sub-2.0 nm islands using cetyltrimethylammoniumchloride (CTAC) and citric acid as surfactant and reductant, respectively (Fig. S1 (ESI†)). Interestingly, by adjusting the ratio of Pd to Pt precursors, the composition of PdPt alloyed nanocrystals can be tuned. More importantly, the as-synthesized $Pd_{50}Pt_{50}$ nanoalloys exhibit much higher electrocatalytic activity and durability for methanol oxidation than commercial Pt catalysts.

Fig. 1(a), Fig. S2a ((ESI†) and Fig. 1(b) show the representative transmission electron microscopic (TEM) and the high-angle annular dark-field scanning transmission electron microscope (HAADF-STEM) images, respectively, of the as-synthesized $Pd_{50}Pt_{50}$ sample (the feeding molar ratio of H_2PtCl_6 to Na_2PdCl_4 is 1:1. The sample is marked as $Pd_{50}Pt_{50}$). The ICP-OES analysis also indicates that the atomic ratios of Pd and Pt are in agreement with the feed ratio of metal precursors (Table S1 (ESI†)), which represents the complete reduction of the reaction (Fig. S1 (ESI†)). As can be seen, the product consists of a large quantity of uniform particles and the average diameter of particles is about 35 ± 2.0 nm. Moreover, many ultrasmall islands distribute on the surface. The high-resolution TEM (HRTEM) image of a single particle is shown in Fig. 1(c). The well-resolved lattice fringes are clearly observed in the whole particle and the lattice orientation of ultrasmall islands is the same as host particle, which implies the whole particle is a single crystal and it is also proven by the corresponding FT pattern (Fig. 1c). The interval between two lattice fringes was measured to be 0.22 nm, closed to the (111) lattice spacing of the face-centered cubic (*fcc*) Pd/Pt. As shown in Fig. 1(d) and Fig. S2b (ESI†), the lateral length of ultrasmall islands is below 2.0 nm, about 1.75 ±0.3 nm. It means that sub-2.0 nm islands can be successfully acquired by our current aqueous method. More importantly, these PdPt nanoalloys with sub-2.0 nm islands contain many steps, corners and

boundaries (Fig. 1c, 1d and Fig. S2b (ESI†)), which can act as highly catalytic active sites in catalytic reaction.[21-24, 25]

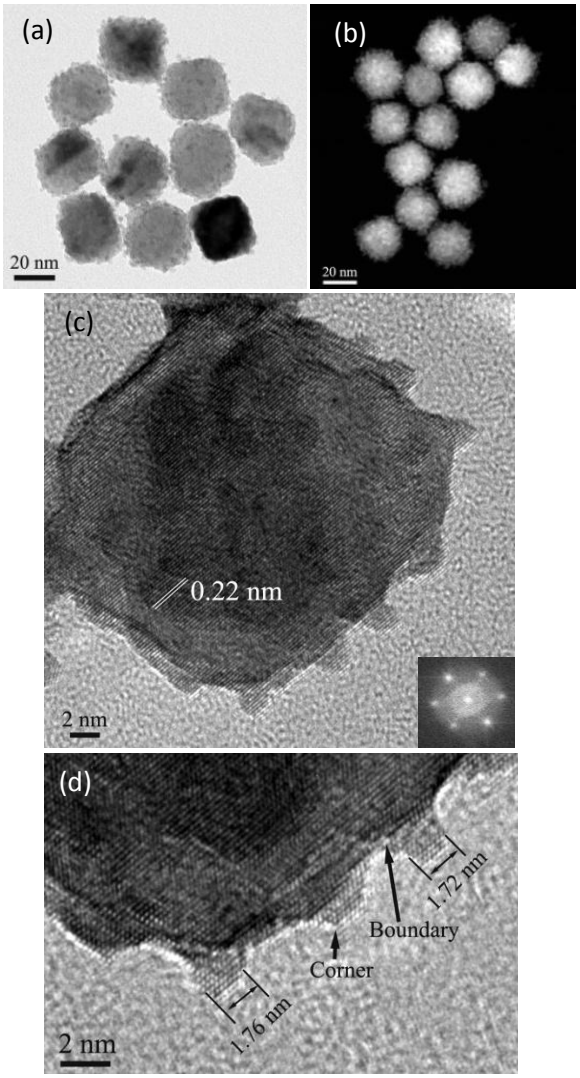

Fig.1 TEM (a), HADDF-STEM (b) and HRTEM (c, d) images of as-synthesized $Pd_{50}Pt_{50}$ nanoalloys with sub-2.0 nm islands. (The inset in (c) is the corresponding FT pattern.)

The X-ray diffraction (XRD) pattern (Fig.2a) of the as-synthesized product shows five peaks corresponding to (111), (200), (220), (311) and (222) of *fcc* Pd/Pt (Pd: JCPDS-65-2867; Pt: JCPDS-65-2868). Moreover, the energy dispersive X-ray (EDX) spectra also reveal the product is made of Pt and Pd (Fig. 2b). The positional distribution of Pd and Pt in the $Pd_{50}Pt_{50}$ nanoalloys was revealed by EDX line-scan analysis and element analysis mapping. Fig. 2c-f show Pd and Pt uniformly distribute in the whole particle, which indicates the as-synthesized nanoparticle is alloy structure. It is well known that Pd and Pt very easily form alloy through the co-reduction of Pd and Pt salts in the solution phase because they have a very small lattice mismatch of only 0.77% and similar redox potential ($PdCl_4^{2-}$/Pd (0.62 V versus RHE); $PtCl_6^{2-}$/Pt (0.74 V versus RHE)). Furthermore, the composition of the PdPt nanoalloys with sub-2.0 nm islands can be tuned by changing the molar ratio of metal salts of Pd and Pt (Fig. S3 (ESI†)).

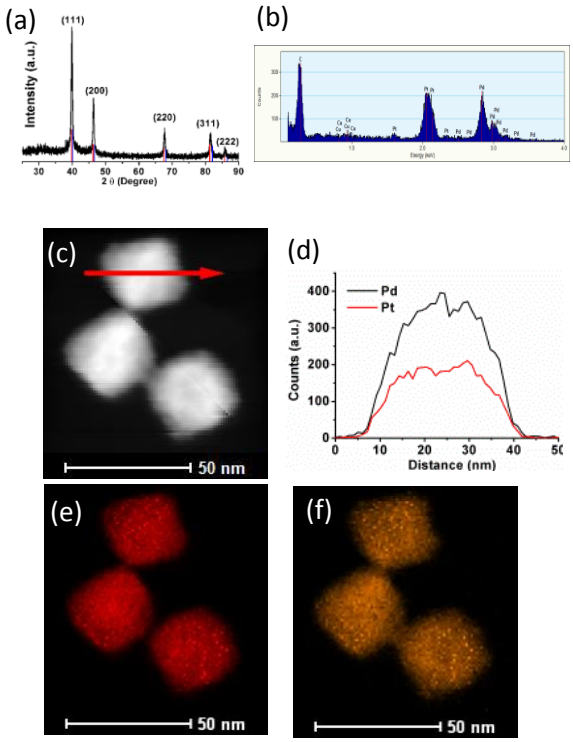

Fig.2 XRD pattern (a), EDX spectra (b), HADDF-STEM images (c), the corresponding EDX line scanning profiles (d) and elemental maps (e) Pd (Red) and (f) Pt (Golden yellow) of as-synthesized $Pd_{50}Pt_{50}$ bimetallic nanocrystals with sub-2.0 nm islands. (The red and the blue in XRD pattern stand for the standard peaks for Pd and Pt, respectively).

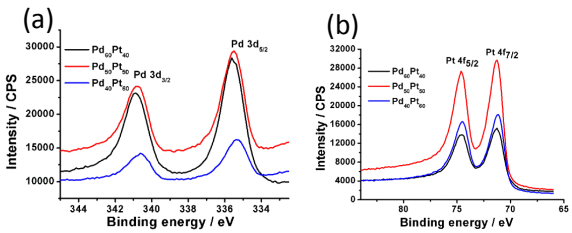

Fig. 3 XPS of as-synthesized PdPt nanoalloys with sub-2.0 nm islands. (a) Pd 3d region; (b) Pt 4f region.

Generally, the catalytic activity is more determined by the composition of surface (the outmost layer) or near-surface of catalyst. Therefore, we checked the near-surface composition by X-ray photoelectron spectroscopy (XPS) that can probe the region of a few nanometers within the surface.[26, 27] Fig. 3a and 3b show the XPS spectra of Pd 3d and Pt 4f for the as-synthesized dendrite-like PdPt nanoalloys. The $3d_{5/2}$ and $3d_{3/2}$ peaks at about 335.4 and 340.7 eV are attributed to metallic Pd (Fig. 3a). The $4f_{7/2}$ and $4f_{5/2}$ peaks at about 71.2 and 74.5 eV are attributed to metallic Pt (Fig. 3b). The Pd : Pt atomic percentage of samples is determined by combining the integrated area with sensitivity factors of Pd 3d and Pt 4f.[27, 29] They are 61.7 : 38.3, 51.3 : 48.7 and 41.6 : 58.4 for sample $Pd_{60}Pt_{40}$, $Pd_{50}Pt_{50}$ and $Pd_{40}Pt_{60}$, respectively, which is consistent with the feeding ratio of Pd and Pt and also revealing complete reduction of Pd^{2+} and Pt^{4+} species in our synthesis.

The catalytic performance of the PdPt alloyed nanocrystals with sub-2.0 nm islands toward methanol oxidation reaction (MOR) was tested with three-electrode system in the nitrogen saturated electrolytes of 0.1 M $HClO_4$ and 0.1 M CH_3OH at a scan rate of 50 mV/s at room temperature (25 ℃). For comparison, the catalytic performance of the commercial Pt black was also tested. All current density values were normalized to the electrochemically active surface area (ECSA) estimated from the hydrogen adsorption-desorption charges (Fig. S4 (ESI†)), which is correspond to the intrinsic catalytic activity of the catalyst. The initial cyclic voltammetric curves (CVs) are shown in Fig.4 (a).The PdPt alloyed nanocrystals demonstrated a composition-dependent catalytic performance toward MOR. The peak current density of $Pd_{60}Pt_{40}$, $Pd_{40}Pt_{60}$ and $Pd_{50}Pt_{50}$ is respectively 0.35, 0.79 and 1.08 mA cm^{-2}. And the $Pd_{50}Pt_{50}$ nanoalloys show the best performance, which may be ascribed to the electronic coupling between Pd and Pt metals and the electronic coupling could be optimized when the atomic percentage of Pt is ~ 50%.[21, 29, 30] It is well known that MOR is a structure-sensitive reaction[9, 31] and thus the change of surface atom arrangements of bimetallic PdPt nanocrystals easily leads to the activity change for MOR although they have the same shape and the same size. Compared to commercial Pt black, the peak current density on the $Pd_{50}Pt_{50}$ nanoalloys is 2.03 times that on the commercial Pt black (0.53 mA cm^{-2}). The enhancement in electrocatalytic activity for the $Pd_{50}Pt_{50}$ bimetallic nanoalloys with sub-2.0 nm islands may be ascribed to the many corners, edges and boundaries existing in the surface of the unique structure (Fig. 1a-d) together with the synergistic effect originating from the coexistence of surface Pd and Pt atoms.[30, 32]

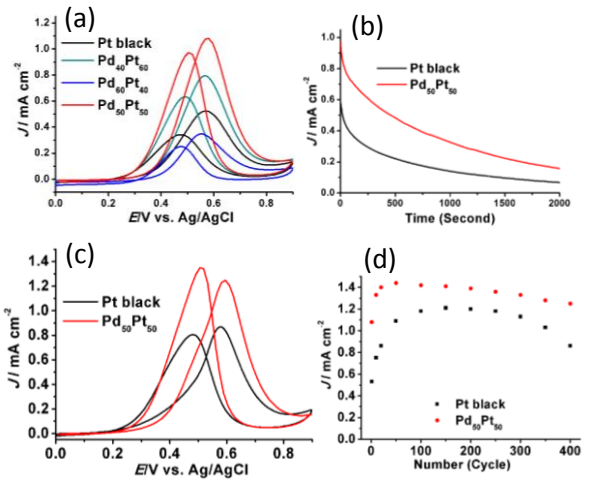

Fig. 4 The initial cyclic voltammetric curves (CVs) of as-synthesized PdPt nanoalloys with sub-2.0 nm islands and commercial Pt black. (a) Specific activity in 0.1M CH_3OH + 0.1 M $HClO_4$ solution; (b) Current~time curves of methanol oxidation on $Pd_{50}Pt_{50}$ nanoalloys and commercial Pt black in 0.1 M CH_3OH + 0.1 M $HClO_4$ solution at 0.5 V for 2000 s; (c) The 400th CVs of $Pd_{50}Pt_{50}$ nanoalloys and commercial Pt black; (d) The durability performance of $Pd_{50}Pt_{50}$ nanoalloys and commercial Pt black in 0.1 M CH_3OH + 0.1 M $HClO_4$ solution.

The stability of the $Pd_{50}Pt_{50}$ nanoalloys with sub-2.0 nm islands and the commercial Pt black has also been investigated. The obtained current-time curves recorded at 0.5 V for 2000 s are shown in Fig.4 (b). We can see, after 2000s, the current density value on the $Pd_{50}Pt_{50}$ nanoalloys (0.16 mA cm^{-2}) is much higher than that on commercial Pt black (0.070 mA cm^{-2}), which implies that the $Pd_{50}Pt_{50}$ nanoalloys have better stability. In order to further confirm it, the durability of the as-synthesized $Pd_{50}Pt_{50}$ nanoalloys with sub-2.0 nm islands and commercial Pt black were tested by repeating the CV for 400 cycles in 0.1 M $HClO_4$ + 0.1 M CH_3OH and 800 cycles in 0.1 M $HClO_4$ + 0.5 M CH_3OH. After 400 cycles, the current density value of the $Pd_{50}Pt_{50}$ nanoalloys remained much higher than that of the commercial Pt black (Fig.4c), they are 1.25 and 0.86 mA cm^{-2}, respectively. Relative to the maximum current density value (1.44 mA cm^{-2} for the $Pd_{50}Pt_{50}$ nanoalloy; 1.21 mA cm^{-2} for commercial Pt black. (Fig. 4d, Fig. S5a-b) (ESI†)), the loss of activity of the $Pd_{50}Pt_{50}$ nanoalloys and the commercial Pt black is 13.2% and 28.9%, respectively (Fig.4d). It shows that the $Pd_{50}Pt_{50}$ nanoalloys have a higher durability than the commercial Pt black. Significantly, after 400 cycles, the remaining mass density value over the $Pd_{50}Pt_{50}$ nanoalloys is a little higher than the maximum value over the commercial Pt black, they are 1.25 to 1.21 mA cm^{-2} (Fig. 4d). It was further confirmed by repeating the CV for 800 cycles with higher methanol concentration (0.5 M) (Fig. S5c-d and Fig. S6 (ESI†)). After 800 cycles, the loss of activity of the $Pd_{50}Pt_{50}$ nanoalloys is 33.3% (1.88mA cm^{-2} after 800 cycles; the maximum: 2.82 mA cm^{-2}); the loss of activity of commercial Pt black is 48.5% (1.03mA cm^{-2}after 800 cycles; the maximum: 2.0mA cm^{-2}). The reason for the better durability of the $Pd_{50}Pt_{50}$ nanoalloys may be ascribed to the more durable nature of the (111) facet of PdPt bimetallic nanoalloys and the synergetic effect of the Pd and Pt atoms, which has been reported in the MOR with PdPt bimetallic nanoalloys as electrocatalysts.[7, 32]

In conclusion, the high-yield, composition-tunable PdPt nanoalloys with Sub-2.0 nm islands were firstly achieved through a facile aqueous approach. These PdPt nanoalloys demonstrated a composition-dependent electrocatalytic activity toward methanol oxidation. Among them, the $Pd_{50}Pt_{50}$ displayed the highest catalytic performance. Due to the special structure and modified electronic structure, the $Pd_{50}Pt_{50}$ nanoalloys exhibited a remarkable catalytic activity and durability. This research may not only provide a simple and convenient approach to synthesize novelty PdPt nanoalloyed structures as highly active and highly durable catalysts for direct methanol fuel cells, but also enable the potential applications of PdPt nanoalloys for various chemical reactions such as CO oxidation reaction and hydrogenation of aromatic hydrocarbons.

This work is supported by the NSFC (21361005 and 21373175), Foundation for the Talents by the Guizhou University (X060025), Natural Science Foundation of Guizhou Province (20072013), and Fundamental Research Funds for the Central Universities (2012121019).

Notes and references

[a] Department of Chemistry, College of Chemistry and Chemical Engineering,Guizhou University, Guiyang, Guizhou province 550025, P. R. China. E-mail: sci.qyuan@gzu.edu.cn
[b] State Key Laboratory of Physical Chemistry of Solid Surfaces, College of Chemistry and Chemical Engineering, Xiamen University, Xiamen, 361005, P. R. China.E-mail:zhouzy@xmu.edu.cn
†Electronic Supplementary Information (ESI) available: *Experimental details, Digital photos, TEM, and CVs.See http://dx.doi.org/10.1039/b000000x/*

1 N. S. Porter, H. Wu, Z. Quan, J. Fang, *Acc. Chem. Res*, 2013, **46**, 1867.
2 J. Rossmeisl, P. Ferrin, G. A. Tritsaris, A. U. Nilekar, S. Koh, S. E. Bae, S. R. Brankovic, P. Strasser and M. Mavrikakis, *Energy Environ. Sci.*, 2012, **5**, 8335.

3 X. Zhao, M. Yin, L. Ma, L. Liang, C. Liu, J. Liao, T. Lu, W. Xing, *Energy Environ. Sci.*, 2011, **4**, 2736.
4 A.Yin, X. Min, Y. W. Zhang and C. H. Yan, *J. Am. Chem. Soc.*, 2011,**133**, 3816.
5 Y. Kang, J. Beom Pyo, X. Ye, T. R. Gordon and C. B. Murray, *ACS Nano*, 2012, **6**, 5642.
6 H. Yang, J. Zhang, K. Sun, S. Zou, J. Y.Fang, *Angew. Chem. Int. Ed.*, 2010, **49**, 6848.
7 Y. Liu, M. Chi, V. Mazumder, K. L. More, S. Soled, J. D. Henao, S. H. Sun, *Chem. Mater.*, 2011, **23**, 4199.
8 C. Poh, Z. Tian, J. Gao, Z. Liu, J. Lin, Y. P. Feng and F. Su, *J. Mater. Chem.*, 2012, **22**, 13643.
9 X. Liu, C. Cui, M. Gong, H. Li, Y. Xue, F. Fan, S. H. Yu, *Chem. Commun.*, 2013, **49**, 8704.
10 Y. Qi, T. Bian, S. Choi, Y. Jiang, C. Jin, M. Fu, H. Zhang, D. Yang, *Chem. Commun.*, 2014, **50**, 560.
11 B. Y. Xia, H. B. Wu, X. Wang, X. W. Lou, *J. Am. Chem. Soc.*, 2012, **134**, 13934.
12 N. T. Khi, J. Yoon, H. Kim, S. Lee, B. Kim, H. Baik, S. J. Kwon and K. Lee, *Nanoscale*, 2013, **5**, 5738.
13 V. Stamenkovic, B. S. Mun, K. J. J. Mayrhofer, P. N. Ross,N. Markovic, J. Rossmeisl, J. Greeley and J. K. Nskov, *Angew. Chem. Int. Ed.*, 2006, **45**, 2897.
14 Q. Yuan, D.-B. Huang, H.-H. Wang, Z.-Y. Zhou, Q. Wang, *CrystEngComm*, 2014, **16**, 2560.
15 Z. Zhang , Y. Yang , F. Nosheen , P. Wang , J. Zhang , J. Zhuang , X. Wang, *small*, 2013, **9**, 3063.
16 S. Alayoglu, A. U. Nilekar, M. Mavrikakis, B. Eichhorn, *Nat. Mater.*, 2008, **7**, 333.
17 Q. Liu, Z. Yan, N. L. Henderson, J. C. Dauer, D. W. Goodman, J. D. Batteas, R. E. Schaak, *J. Am. Chem. Soc.*, 2009, **131**, 5720.
18 Q. Yuan, Z. Zhou, J. Zhuang and X. Wang, *Chem. Commun.*, 2010, **46**, 1491.
19 D. Xu, Z. Liu, H. Yang, Q. Liu, J. Zhang, J. Fang, S. Zou, K. Sun, *Angew. Chem. Int. Ed.*, 2009, **48**, 4217.
20 Z. Zhou, X. Kang, Y. Song, S. Chen, *Chem. Commun.*, 2012, **48**, 3391.
21 B. Lim, M. J. Jiang, P. H. C. Camargo, E. C. Cho, J. Tao, X. M. Lu, Y. M. Zhu, Y. N. Xia, Science, 2009, **324**, 1302.
22 Z. M. Peng, H. Yang, J. Am. Chem. Soc., 2009, **131**, 7542.
23 L. Wang, Y. Nemoto, Y. Yamauchi, *J. Am. Chem. Soc.*, 2011, **133**, 9674.
24 J. Lv, J. Zheng, S. Li, L. Chen, A. Wang, J. Feng, *J. Mater. Chem. A*, 2014, **2**, 4384.
25 H. Lee, S. E. Habas, G. A. Somorjai, P. Yang, *J. Am. Chem. Soc.*, 2008, **130**, 5406.
26 F. Tao, M. E. Grass, Y. W. Zhang, D. R. Butcher, J. R. Renzas, Z. Liu, J. Y. Chung, B. S. Mun, M. Salmeron, G. A. Somorjai, *Science*, 2008, **322**, 932.
27 Y. Deng, N. Tian, Z. Zhou, R. Huang, Z. Liu, J. Xiao, S. Sun, *Chem. Sci.*, 2012, **3**, 1157.
28 C. D. Wagner, L. E. Davis, M. V. Zeller, J. A. Taylor, R. H. Raymond and L. H. Gale, *Surf. Interface Anal.*, 1981, **3**, 211.
29 W. P. Zhou, X. F. Yang, M. B. Vukmirovic, B. E. Koel, J. Jiao, G. W. Peng, M. Mavrikakis, R. R. Adzic, *J. Am. Chem. Soc.*, 2009, **131**, 12755.
30 X. Huang, Y. Li, Y. Li, H. Zhou, X. Duan and Y.Huang, *Nano Lett*., 2012, **12**, 4265.
31 N. P. Lebedeva, A. Rodes, J. M. Feliu, M. T. M. Koper and R. A. van Santen, *J. Phys. Chem. B*, 2002, **106**, 9863.
32 A. Yin, X. Min, Y. W. Zhang, C. H. Yan, *J. Am. Chem. Soc.*, 2011, **133**, 3816.